Build Simul (2024) 17: 1401–1417
https://doi.org/10.1007/s12273-024-1147-0

Application-driven development of a thermal imaging-based cabin occupant thermal sensation assessment model and its validation

Junmeng Lyu, Yuxin Yang, Yongxiang Shi, Zhiwei Lian (✉)

Department of Architecture, School of Design, Shanghai Jiao Tong University, Shanghai, China

Abstract

The air conditioning (A/C) of cabins allows for customized control, but manual adjustments may distract drivers, as well as result in energy inefficiency. Several existing thermal sensation models require complex inputs, which are challenging to gather whilst driving. To address this issue, this study developed a non-contact thermal sensation model for cabin occupants based on thermal imaging sensor. To collect actual data used for modeling, an outdoor subject experiment was conducted. In this study, initial training was conducted to compare the performance of six algorithms in building the model, with random forests algorithm showing the best performance. Besides, this study employed the recursive feature elimination (RFE) method with cross-validation algorithm for identifying the key features. In the end, the model was retrained using the selected features. The model that incorporated both environmental parameters and facial-temperature features demonstrated the best performance, with an R^2 of 0.659 on the test set. Eliminating the hard-to-measure windshield surface temperature resulted in a slight reduction in accuracy, yielding an R^2 of 0.651. To verify the generalizability of the model, this study further conducted independent validation experiments. The selected model, which exhibited a mean absolute error (MAE) of less than 0.4 in thermal sensation units, was proven to be highly applicable. The results can offer new solutions for automatic control of cabin A/C.

Keywords

model
assessment
thermal imaging
vehicle air conditioner
thermal sensation
transient cabin indoor environment

Article History

Received: 22 February 2024
Revised: 09 April 2024
Accepted: 16 May 2024

1 Introduction

Modern automobiles are now charged with a dual mission: Not only should they offer commuting convenience to their occupants, but they are also supposed to elevate passenger comfort, while concurrently curbing energy consumption (de Santis et al. 2022).

Presently, the regulation of the thermal environment within the vehicle cabin primarily relies on the intentional manipulation of the air conditioning (A/C) system. While this mode of control gives users the freedom to tailor their preferred temperature settings, it does come with certain disadvantages. Although it allows the driver to adjust the A/C settings while in transit, the driving experience could be impacted due to potential safety concerns caused by distraction. Furthermore, fixed A/C configurations with irrational adjustments could result in energy inefficiencies. Incorporating real-time monitoring technology to track occupant thermal sensation within the vehicle's A/C system enables us to not only meet occupants' thermal requirements more effectively, but also optimize energy consumption. Employing a logical operational framework to achieve automated and intelligent regulation of the cabin's thermal environment will bring about a mutually-beneficial outcome, enhancing both occupant comfort and energy efficiency.

In contrast to the well-established models for evaluating thermal sensation within building environments, the models for cabin environments remain somewhat nebulous (refer to Table 1). Since the cabin environment is characterized by dynamics and non-uniformity, thermal sensation models developed for dynamic environments, such as the dynamic thermal sensation (DTS) model by Fiala et al. (2003) and the model proposed by Lai et al. (2017), are often applied directly to cabin environments. Neither of these models

E-mail: zwlian@sjtu.edu.cn

List of symbols

$dT_{sk,i}/dt$	change rate of skin temperature at region i (°C/min)
RH	relative humidity (%)
SE	solar elevation angle (°)
SR	solar radiation intensity (W/m^2)
T_0	initial cabin air temperature (°C)
T_A	air temperature (°C)
$T_{Cheek(out)}$	window side cheek skin temperature (°C)
$T_{Cheek(in)}$	non-window side cheek skin temperature (°C)
T_{ED}	range of the skin temperature differences between facial regions (°C)
$T_{Forehead}$	forehead skin temperature (°C)
T_{FW}	surface temperature of front windshield (°C)
T_{LBW}	surface temperature of back row left window (°C)
T_{LFW}	surface temperature of front row left window (°C)
T_{Max}	the maximum skin temperature of facial regions (°C)
T_{Min}	the minimum skin temperature of facial regions (°C)
T_{Nose}	nose skin temperature (°C)
T_{RFW}	surface temperature of front row right window (°C)
$T_{sk,m}$	mean skin temperature (°C)
T_{STD}	standard deviation of the skin temperature differences between facial regions (°C)
$T_{Supply,1}$	No. 1 vent air supply temperature (°C)
$T_{Supply,2}$	No. 2 vent air supply temperature (°C)
V_{air}	air velocity (m/s)

Abbreviations

A/C	air conditioning
DTR	decision tree regression
ENR	elastic net regression
LassoR	least absolute shrinkage and selection operator regression
LR	linear regression
MAE	mean absolute error
MSE	mean squared error
RFE	recursive feature elimination
RFR	random forest regression
RidgeR	ridge regression
TSV	thermal sensation vote

was specifically designed for cabin environments. Guan et al. (2003a, 2003b) utilized physiological inputs such as the thermal load and its change rate, along with skin temperature and its change rate, to conduct thermal sensation calculations. Although this model was developed specifically for cabin environments, there are not that many studies that further assess its performance. The University of California, Berkeley (UCB) has developed a thermal sensation assessment model that targets cabin environments by leveraging local skin temperature, core temperature, and the rates of change in both skin and core temperature (Zhang 2003). Given its capability to predict thermal sensation via a coupled thermo-physiological model, and its development based on cabin environments, the UCB model is the fundament for most existing cabin thermal comfort assessments. However, as research into transient thermal comfort under dynamic environmental conditions has advanced, certain studies have raised concerns about the errors of the UCB model. Building upon these observations, Zhou et al. (2020) introduced a novel model designed for transient, non-uniform cabin environments. Compared to the UCB model, Zhou's model demonstrates superior assessment accuracy.

Overall, existing research on thermal sensation models of cabin environments primarily focuses on performance optimization and modifications within the traditional framework. Despite incorporating more inputs to enhance computational accuracy in complex cabin environments, these models are still limited in the sense of practical application. On the one hand, such models often require multifaceted inputs like multi-segmented skin temperatures, mean skin temperature, and even core temperature, which are challenging to obtain during actual driving. On the other hand, the fundamental thermal equilibrium and thermo-physiology models impose strict assumptions, failing to offer precise feedback on individual thermal sensation. These thermal sensation models often support thermal environment optimization during the cabin design stage through coupled simulation. However, it is impractical to use these models to identify real-time thermal sensations of individuals and adjust air conditioner setpoints automatically during actual driving. He et al. (2023b) used machine learning algorithm to predict environmental parameters and further utilized the Fanger's PMV (predicted mean vote) model (Fanger 1970) to output the thermal sensations of the occupants. Although this study provides insights into the automatic control of air conditioner from the perspective of practical application, the PMV model is not suitable for evaluating dynamic, non-uniform, and non-neutral environments because it is established on experiments conducted under steady-state conditions (Lian 2024).

Table 1 Some studies related to cabin thermal comfort

Model name	Model input	Notes
DTS model (Fiala et al. 2003)	$\Delta T_{sk,m}$, $\frac{dT^{(-)}_{sk,m}}{dt}$, $\frac{dT^{(+)}_{sk,m}}{dt_{max}}$, ΔT_{hy}	Applicable for both transient and steady-state environments. Physiological parameters are calculated based on the Fiala thermo-physiological model, followed by the calculation of thermal sensation.
Lai's model (Lai et al. 2017)	TL, $T_{sk,m}$, $\frac{dT_{sk,m}}{dt}$	Applicable for outdoor transient environments.
Guan's model (Guan et al. 2003a, 2003b)	Q_{net}, $T_{sk,m}$, $T_{sk,n}$, $\frac{dT_{sk,m}}{dt}$	Applicable for both transient and steady-state cabin environments.
UCB model (Arens et al. 2006a, 2006b; Zhang et al. 2010a, 2010b)	$\Delta T_{sk,m}$, $\Delta T_{sk,i}$, $\frac{dT_{sk,i}}{dt}$, $\frac{dT_{cr}}{dt}$	Applicable for non-uniform environments. Using the thermo-physiological model, skin temperature and local thermal sensation are determined for non-uniform environments to calculate overall thermal comfort.
Zhou's model (Zhou et al. 2020)	$TL_{g(face)}$, $TL_{s(face)}$, $T_{sk,m}$, T_{out}	Applicable for both transient and steady-state cabin environments.
Li's model (Li et al. 2022)	T_{head}, T_{trunk}, T_{back}, T_{arm}, T_{hand}, T_{leg}, T_{foot}	Established based on transient and steady-state environmental experiments.
He's model (He et al. 2023b)	T_{out}, T_{air_return}, RH, SR, T_{air_supply}, V_{air}	Established based on transient environmental experiments. The zonal temperature is determined using A/C and outdoor parameters, followed by PMV calculation.

$\Delta T_{sk,m}$ is the difference in mean skin temperature under neutral thermal sensation and current status; $\frac{dT^{(-)}_{sk,m}}{dt}$ is negative change rate of the mean skin temperature; $\frac{dT^{(+)}_{sk,m}}{dt_{max}}$ is the maximum positive change rate of skin temperature; ΔT_{hy} is the difference in head core temperature under neutral thermal sensation and current situation.

TL is thermal load; $T_{sk,m}$ is mean skin temperature; $\frac{dT_{sk,m}}{dt}$ is change rate of the mean skin temperature.

Q_{net} is the rate of heat gain; $T_{sk,n}$ is instantaneous neutral skin temperature.

$\Delta T_{sk,i}$ is local skin temperature; $\frac{dT_{sk,i}}{dt}$ is the change rate of local skin temperature; $\frac{dT_{cr}}{dt}$ is the change rate of core temperature.

$TL_{g(face)}$ is the thermal load of face that changes gradually; $TL_{s(face)}$ is the thermal load of face that changes suddenly; T_{out} is outdoor air temperature.

T_{head} is skin temperature of the head; T_{trunk} is skin temperature of the trunk; T_{back} is skin temperature of the back; T_{arm} is skin temperature of the arm; T_{hand} is skin temperature of the hand; T_{leg} is skin temperature of the leg; T_{foot} is skin temperature of the foot.

T_{air_return} is air return temperature; RH is the relative humidity; SR is solar radiation; T_{air_supply} is air supply temperature; V_{air} is air velocity.

The perception of temperature by the human body is achieved through the thermo-receptors located beneath the skin, which transmit signals to the hypothalamus via the sympathetic nervous system (Nadel et al. 1971). Existing researches have pointed out that the skin temperature of specific body parts, such as the wrist (Choi and Loftness 2012) and the forearm (Zhao et al. 2023), is closely associated with human thermal sensation. Building upon these theoretical foundations, scholars have employed physiological sensors to collect skin temperature data, thereby constructing thermal sensation models. Considering that non-invasive measurement methods can minimize disruptions to the activities of tested individuals (Yang et al. 2019, 2020), the use of thermal imaging sensors to measure and extract skin temperatures at specific parts, followed by assessments of thermal sensation, has emerged as a prevailing trend in the field of intelligent thermal environment design. Cosma and Simha (2018) harnessed a pioneering fusion of sensors and visual perception systems to extract temperature information from subjects' skin and clothing. Building on chamber experimental datasets, He et al. (2023a) proposed an approach to predict occupant thermal state using a combination of infrared thermography and computer vision, achieving over 70% accuracy on independent data sets. Since the facial region is rarely covered by clothing, capturing facial skin temperature with infrared thermography is simple and feasible. Li et al. (2018, 2019) proposed a real-time thermal preference prediction framework employing infrared thermography. By aggregating features collected from various facial regions, this framework demonstrates an impressive accuracy of 85% in predicting subjects' thermal preferences. Lyu et al. (2023) introduced a two-stage thermal sensation assessment framework founded on infrared thermography. By collecting data on cheek skin temperatures, air velocity, air temperature, and facial skin temperature uniformity, this framework enables

the assessment of steady-state human thermal sensation, with a mean absolute error (MAE) below 0.5 in thermal sensation units. Wu and Cao (2022) utilized facial skin temperature data recorded via thermography as input parameters to compare the performance of various data-driven algorithms in thermal sensation prediction. Subsequently, they applied the model to the automated control of household A/C systems, achieving notably high accuracy (Wu et al. 2023a).

However, these models are primarily developed based on built indoor environments. In contrast, vehicle cabins are significantly influenced by dynamic factors such as solar radiation. Furthermore, due to the weaker thermal insulation properties of the outer walls of vehicle cabins and the larger transparent enclosure area, changes in outdoor weather can lead to more pronounced variations in the thermal environment within the vehicle cabin compared to that of the built indoor environments (Sun et al. 2023). Additionally, the non-uniformity of the cabin environment and the more complex heat transfer processes between occupants and the cabin thermal environment may lead to unique quantitative relationships between facial skin temperature and thermal sensation. Therefore, when evaluating occupant thermal sensation within the transient, non-uniform thermal environment of a vehicle cabin, it is imperative to consider a multitude of factors. It may be unreasonable to apply thermal sensation assessment models, which are essentially established for built indoor environments, to cabin environments (Lai et al. 2020).

To address these limitations, this study aims to develop a facial thermal imaging-based thermal sensation assessment model for cabin occupants. By integrating this model into the automotive A/C control logic, automatic adjustments to A/C settings can be made to meet the thermal demands of the occupants. To this end, experiments were conducted on subjects in a vehicle cabin parked outdoors. During the experiments, environmental parameters including air temperature, surface temperature, relative humidity, and solar radiation intensity were monitored. Subjective feedback on thermal sensation was collected through questionnaires, and the facial skin temperatures of the subjects were captured using an infrared thermography. Based on the dataset obtained, initial model training was conducted to select the best algorithm from six regression algorithms. Additionally, recursive feature elimination (RFE) with cross-validation algorithm was employed for feature selection. The selected features were then applied to retrain the model using the optimal algorithm chosen, and independent validation experiments were conducted to test the generalizability and accuracy of the model under practical conditions.

2 Methodology

2.1 Development of model

This study aims to establish a thermal sensation model for cabin drivers and passengers. Figure 1 shows the model development process, which includes 8 modules (model data acquisition, feature grouping, algorithm comparison, initial model training, feature selection, model retraining, model output, and model validation). This study uses Python 3.10.6 as the programming language and was implemented on the "Jupyter notebook" editor for model development. The final model is included in the Electronic Supplementary

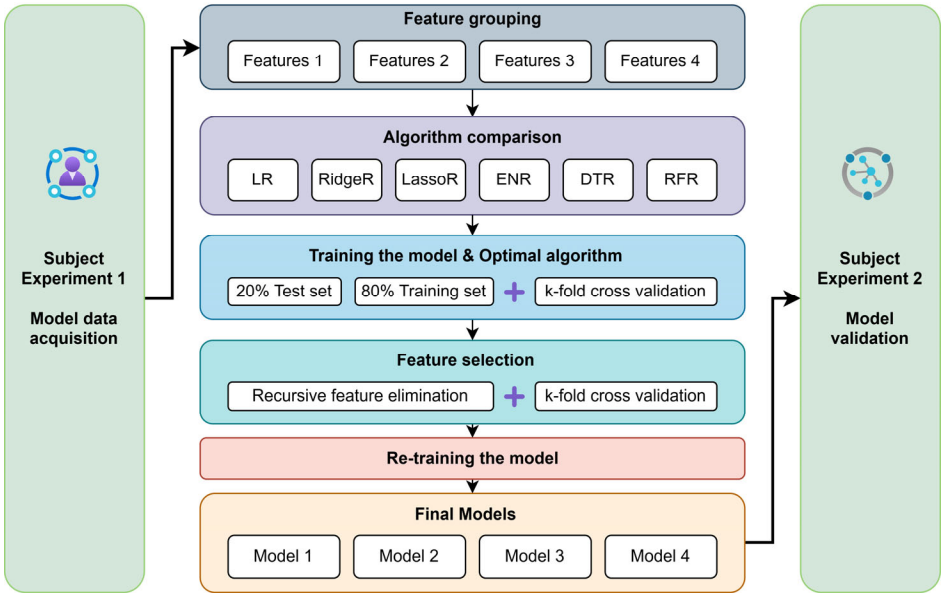

Fig. 1 Model establishment framework

Material (ESM) and can be directly run in a properly configured environment.

2.2 Data collection experiment

To develop a model for assessing the thermal sensation of vehicle cabin occupants, this research involved an experiment designed to gather the required dataset. The experiment was carried out during the summer of 2023, in a vehicle parked outdoors at Shanghai Jiao Tong University.

The experiment replicates the sequence of events commencing as an individual enters an outdoor-parked vehicle and culminating with the activation of the A/C system to achieve a neutral thermal environment. To ensure a wide range of solar radiation intensity within the dataset, experiment was systematically conducted during clear weather periods, specifically in the morning (9:00–11:00), at noon (12:00–14:00), and in the afternoon (15:00–17:00). The initial air temperature range of the vehicle cabin was 36.9 ± 2.1 °C to 54.1 ± 2.8 °C upon subject entering. Nighttime experiments, conducted from 20:00 to 21:00 to simulate conditions without solar radiation, began with an initial air temperature range of 30.7 ± 1.3 °C. After stabilization, the cabin air temperature was maintained at 25.4 ± 1.0 °C, which is within the neutral temperature range defined by ASHRAE-55 (Lan et al. 2022). Considering the varying relative orientations of a car to the sun in real situations, this study adjusted the car's orientation during the daytime to simulate two specific conditions of solar exposure: One is direct sunlight hitting the front windshield, and the other with lateral sunlight irradiation to the cabin (see Figure 2(a)). The nighttime experiments maintained a consistent orientation. Each experimental session involved two subjects, as indicated by the red model in Figure 2(a), along with a member of the research team, represented by the green model in Figure 2(a), who conducted operations within the cabin. Subjects were assigned specific seat numbers, which they were required to retain for all subsequent experimental conditions. Due to the absence of sunlight during nighttime, subjects participated in a single nighttime condition, where both were seated in the front row. All subjects underwent seven experimental sessions. Additionally, considering the restricted space in the cabin and the proximity of subjects to the air conditioner vents, the vents were angled upwards horizontally at 75° to avoid the discomfort of cold draft on occupants. The vehicle's doors and windows remained closed throughout the experiment, and the sunroof and its shade were kept closed. The parameters of the external environment during the experimental period are listed in Table S1 in the ESM.

According to the EN ISO 14505 standard, vehicle thermal comfort experiments should include at least 8 subjects (ISO/TS 2006). In this study, 24 subjects were recruited, comprising 12 males and 12 females. These subjects were university students and a faculty member, with specific details given in Table 2. Subjects were asked to avoid caffeine, alcohol, and intense physical activity before the experiment. Regarding clothing insulation, the mean for female subjects was approximately 0.55 clo, while for males it was 0.49 clo. All subjects signed an informed consent form for the experiment. The experiment received approval from the Science and Technology Ethics Committee of Shanghai Jiao Tong University.

As demonstrated in Figure 2(b), each experiment had a total duration of no less than 62 min. This duration included a pre-experimental adaptation phase lasting at least 20 min

Table 2 Subjects information

	Number	Age	Height (cm)	Weight (kg)
Male	12	23.2 ± 1.6	173.5 ± 5.1	64.5 ± 6.8
Female	12	24.4 ± 2.1	163.5 ± 5.5	54.1 ± 4.8

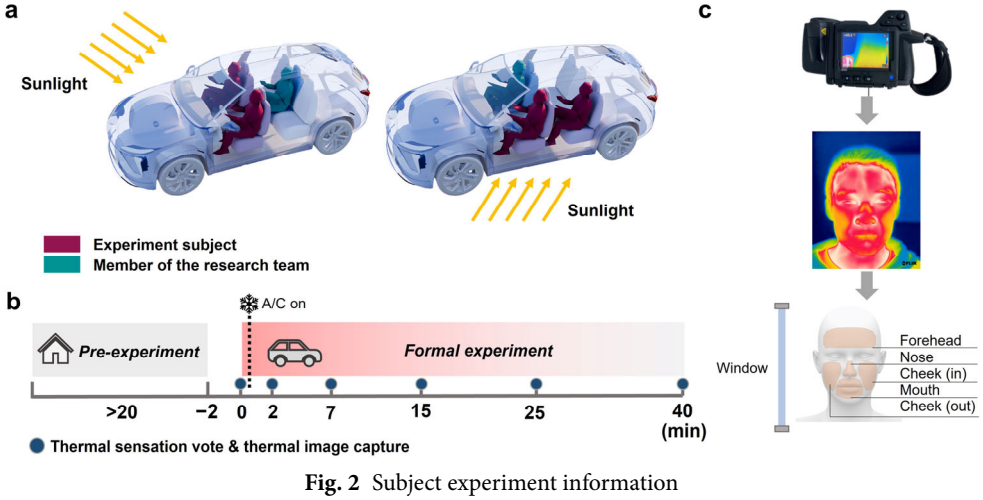

Fig. 2 Subject experiment information

but not exceeding 40 min, a two-minute transition period for moving from outdoors to the cabin, and a 40 min formal experimental session conducted within the cabin. During the adaptation period, subjects stayed in a room with a neutral environment (temperature at 26 °C, air velocity below 0.2 m/s) to attenuate effects of prior thermal experiences. Once the adaptation period was over, subjects moved from the room located on the third floor down the stairs at a normal walking pace to the vehicle outside. Immediately after entering the vehicle, the first thermal sensation questionnaire (ASHRAE 7-point scale) was filled out and a frontal thermal image was taken at a distance of 0.5 m. Following this, the air conditioner was activated and set to "cooling + recirculation" mode. Throughout the experiment, subjects regularly completed thermal sensation votes and underwent facial imaging. Considering safety, subjects remained seated and did not drive during the experiment. Through this experiment, a total of 962 sets of valid sample data from 24 subjects were collected.

In this study, facial skin temperatures were collected using the high-performance FLIR T-460 infrared thermography (FLIR Systems Inc, USA). For details on the collection area, thermography settings, and validation, please refer to previously published paper (Lyu et al. 2023). Due to constraints presented by the infrared thermography's field of view (FOV), the thermography could not be affixed within the vehicle. To guarantee the acquisition of extensive facial thermal imaging data, a trained member of the research team manually conducted thermography from within the cabin. Those involved in this process received specific training to ensure consistency in the imaging procedure. Throughout the experiment, the distance from the thermography to the subjects was rigorously controlled, maintaining a consistent 0.5 meters to meet the necessary resolution and image quality criteria. Figure 2(c) illustrates the precise imaging perspective and the region of skin temperature collection. During the experiment, the air temperature and interior surface temperature inside the cabin were recorded using a thermocouple system (JTNT-A, Jantytech Inc, China) (range: −50 to +120 °C, accuracy: ±0.5 °C). The relative humidity inside the cabin was recorded using a humidity sensor (TR-76ui, T&D Inc, Japan) (range: 10% to 95% RH, accuracy: ±2.5% RH). Specific measurement points and descriptions can be found in Figure S1 and Table S2 in the ESM. A pyranometer (S-LIB-M003, ONSET Inc, USA) was placed horizontally above the dashboard to continuously collect data on solar radiation intensity inside the cabin (spectral range: 300–1,100 nm, measurement range: 0–1,280 W/m², accuracy: ±10 W/m² or ±5%). Monitoring points for external environmental parameters were located 2 meters outside the cabin, providing real-time measurement data for air temperature (S-THB-M002, ONSET Inc, USA, range: from −40 to +75 °C, accuracy: ±0.2°C at 20°C), solar radiation intensity (S-LIB-M003, ONSET Inc, USA, range: 0–1,280 W/m², spectral range: 300–1,100nm, accuracy: ±10 W/m² or ±5%), and relative humidity (S-THB-M002, ONSET Inc, USA, range: 0–100%, accuracy: ±3%).

2.3 Algorithm comparison

In the field of indoor thermal comfort research, machine learning is extensively used (Wu et al. 2018; Shan and Yang 2020; Wang et al. 2020; Zhao et al. 2021; Qavidel Fard et al. 2022). This study, aiming to optimize model performance, applied and compared six basic machine learning regression algorithms: linear regression (LR), ridge regression (RidgeR), lasso regression (LassoR), elastic net regression (ENR), decision tree regression (DTR), and random forest regression (RFR). Linear regression, a fundamental algorithm in statistics, is primarily utilized to estimate the linear relationship between independent and dependent variables. It finds the best fit line by minimizing the sum of squared errors, yet its performance is influenced by the multicollinearity of variables. Ridge regression, suited for datasets with multicollinearity (high correlation among independent variables), improves estimation by adding an L2 regularization term to ordinary linear regression. However, the choice of the regularization coefficient λ significantly affects the model's performance, and the algorithm is sensitive to the scale of features. Lasso regression, a unique form of linear regression, improves the traditional model by introducing an L1 regularization-based penalty term. Different from ridge regression, lasso regression uses L1 regularization, adding a sum of the absolute values of coefficients. This can reduce some coefficients to zero, enabling feature selection. Nevertheless, the choice of λ remains crucial for model performance. Elastic net regression combines ridge and lasso regression, introducing both L1 and L2 regularization terms. It is effective for datasets with multicollinearity or high feature dimensions, though adjusting two regularization parameters for optimal performance can be more complex than single-parameter models. Decision tree regression predicts continuous values by learning simple decision rules from data. Decision tree regression predicts continuous values by learning simple decision rules from data. It typically uses mean squared error (MSE) as the criterion for measurement. This algorithm is highly interpretable and does not require feature scaling, but decision trees are prone to overfitting. The random forest algorithm, based on decision tree algorithms, has been proven effective and robust in the study of thermal comfort and thermal sensation prediction. Overall, a random forest

is a collection of decision trees, whose final decisions are aggregated and weighted into the outcome, effectively avoiding overfitting (Belgiu and Drăguț 2016). It can handle high-dimensional data during training and provides the importance of features. However, its downside is the increased complexity and computational cost of the model. The Scikit-learn library in Python is used to call the required algorithms (Pedregosa et al. 2011).

2.4 Feature selection

Recursive feature elimination (RFE) is a feature selection method based on the wrapper approach, used to select the most important features from the original feature set (Guyon et al. 2002). In each iteration step, RFE trains the model and evaluates the importance of each feature, then eliminates the least contributing feature. This process is repeated on the remaining features until all features have been considered. This backward search method uses a greedy algorithm, starting with the full set of features and progressively removing one feature at a time. The order in which features are eliminated reflects their importance ranking. To enhance the accuracy of the feature selection process, 5-fold cross-validation is combined with the RFE algorithm to form recursive feature elimination with cross-validation (RFECV), which better evaluates the generalization ability of feature subsets on unseen data (Mustaqim et al. 2021).

2.5 Training, testing, and model performance

In the process of developing the model, the "train_test_split" function is used to divide the dataset, allocating 80% as the training set and the remaining 20% as the test set. The "test_size" is set to 0.2, and a random sample's "random_state" is set to 45.

For evaluating the performance of regression models, the MSE calculated by Equation (1) is an indicator of the model's quality, representing the average size of the difference between the model's predictions and the actual observed values. Additionally, the R^2 evaluation metric was introduced, calculated by Equation (2). The R^2 metric is commonly used to evaluate the goodness of fit of a model, focusing on the model's ability to explain the variability in the data. In practice, these two metrics are often used together to comprehensively assess the model's performance. Since the performance of the regression algorithms used is sensitive to hyperparameters, a grid search with 5-fold cross-validation is employed, using R^2 as the metric to find the best combination of hyperparameters. The parameter grid is shown in Table 3.

Table 3 The hyperparameters involved in the optimization

Algorithm	Hyperparameter	Range
RFR	n_estimaters	1 to 20, with an interval of 2
	max_depth	None to 20, with an interval of 2
LR	—	—
RidgeR	alpha	0.1 to 1 with an interval of 0.1 and 1 to 10 with an interval of 1
LassoR	alpha	0.01 to 0.1 with an interval of 0.01 and 0.1 to 1 with an interval of 0.1
ENR	alpha	0.01 to 0.1 with an interval of 0.01 and 0.1 to 1 with an interval of 0.1
	l1_ratio	0.1 to 1, with an interval of 0.1
DTR	—	—

$$\mathrm{MSE} = \frac{1}{n}\sum_{i=1}^{n}\left(Y_i - \hat{Y}_i\right)^2 \tag{1}$$

$$R^2 = 1 - \frac{\sum_{i=1}^{n}\left(Y_i - \hat{Y}_i\right)^2}{\sum_{i=1}^{n}\left(Y_i - \frac{1}{n}\sum_{i=1}^{n}Y_i\right)^2} \tag{2}$$

where n is the number of observations; Y_i is the actual value of the observation; $\hat{Y}_i$ is the predicted value from the model.

After developing the optimal model, this study further analyzed the impact of training set size on model performance, with pseudo-code provided in Figure 3. The size of the test set was fixed at 20% of the dataset to ensure sufficient data for evaluating the model's performance on unseen data. A range of different training set sizes was set, from 10% to 80%, with intervals of 10%. For each specific training set size, the model's MSE and R^2 were calculated using cross-validation methods to assess the model's performance. This method systematically evaluated the impact of different training set sizes on model performance, providing insights into the performance under different training conditions. It also guided best practices for data splitting. The findings help understand how to effectively utilize the best algorithm under specific data constraints to achieve optimal predictive performance.

3 Results

3.1 Data description

The statistical results of interior surface temperature, air temperature, air supply temperature, subject facial skin temperature, solar radiation intensity, and thermal sensation votes in this dataset are given in Figure 4. Thermal sensation

Algorithm 1. Training set size testing

```
# Start of pseudocode

Load the dataset

Define the target variable
Define feature variable

Assign the feature variables and the target variable from the dataset to X and y respectively

Define the trained model

Set a fixed test set size to 20% of the data

Define a series of different training set sizes: from 10% to 80%, in increments of 10%

Create dictionaries results, MSE_errors, R2_errors to store the results

For each training set size:
    Split the dataset into a training set and a test set
    If the current training set size is smaller than the total data minus the test set size:
        Select the corresponding proportion of data as a training subset from the training set
    Otherwise:
        Use all the training set data

    Use 5-fold cross-validation to calculate the mean Mean Squared Error (MSE) and R2 values for the current training subset

    Store the computed mean MSE and R2 values into the results dictionary
    Store the computed standard deviations of MSE and R2 into the MSE_errors and R2_errors dictionaries

# End of pseudocode
```

Fig. 3 Training set size testing pseudo-code

votes and thermal environment data were collected during the dynamic cooling process of a high-temperature cabin. The air temperature (T_A) range in the dataset ranges from 24.2 °C to 57.8 °C. This wide temperature range encompasses various cabin temperature levels occupants might encounter during summer. Correspondingly, the temperature change at the air vent ranges from around 56°C (without A/C on) to about 7 °C (after the air supply temperature stabilizes). The thermal sensation votes primarily focus on neutral and warm sides, with lower voting scores on the cool side, mostly from nighttime conditions. The distribution of votes on the warm side is relatively even, representing the various thermal sensations that occupants might experience inside a cabin during summer without significant imbalance. The range of solar radiation intensity (SR) is from 0 to 487 W/m², with a generally even distribution of daytime samples. The temperature data for transparent surfaces shows a normal distribution at different locations. The mean interior surface temperature of the right front window (T_{RFW}) is 37.7 °C, ranging from 25.5 to 58.2 °C. The left front window displays an interior surface temperature distribution similar to the right front window, but its mean interior surface temperature T_{LFW} was higher than T_{RFW}, ranging from 25.8 to 60.2 °C, due to experimental conditions including lateral sunlight (entering from the left). Compared to the front windows, the windshield has a wider temperature distribution, possibly due to its larger area and direct exposure to solar radiation, with temperatures ranging from 26.3 °C to 69.4 °C.

The facial temperature data of individuals shows a normal distribution. The mean window side cheek skin temperatures ($T_{Cheek(out)}$) and non-window side cheek skin temperatures ($T_{Cheek(in)}$) are 35.7 °C and 35.5 °C, respectively, while the forehead ($T_{Forehead}$) is slightly higher at 35.9°C. The highest is nose skin temperature at 36.1°C, which may be due to its greater exposure to direct sunlight. The skin temperature of peri-oral is similar to that of the window side cheek, with a mean of 35.7 °C, but it has the smallest range of variation, with a standard deviation of 1.0 °C.

Overall, the acquired dataset samples are widely distributed and relatively balanced, capable of covering a variety of thermal environments in the cabin during summer, as well as the thermal sensations and facial skin temperature characteristics experienced by individuals.

3.2 Thermal sensation assessment model—initial model

Features were divided into four groups, as listed in Table 4. These groups are the environmental feature group (Grouping 1), the facial skin temperature information feature group (Grouping 2), the mixed feature group of environmental and facial skin temperature (Grouping 3), and the easily measurable feature group based on practical application (Grouping 4). Compared to the features of

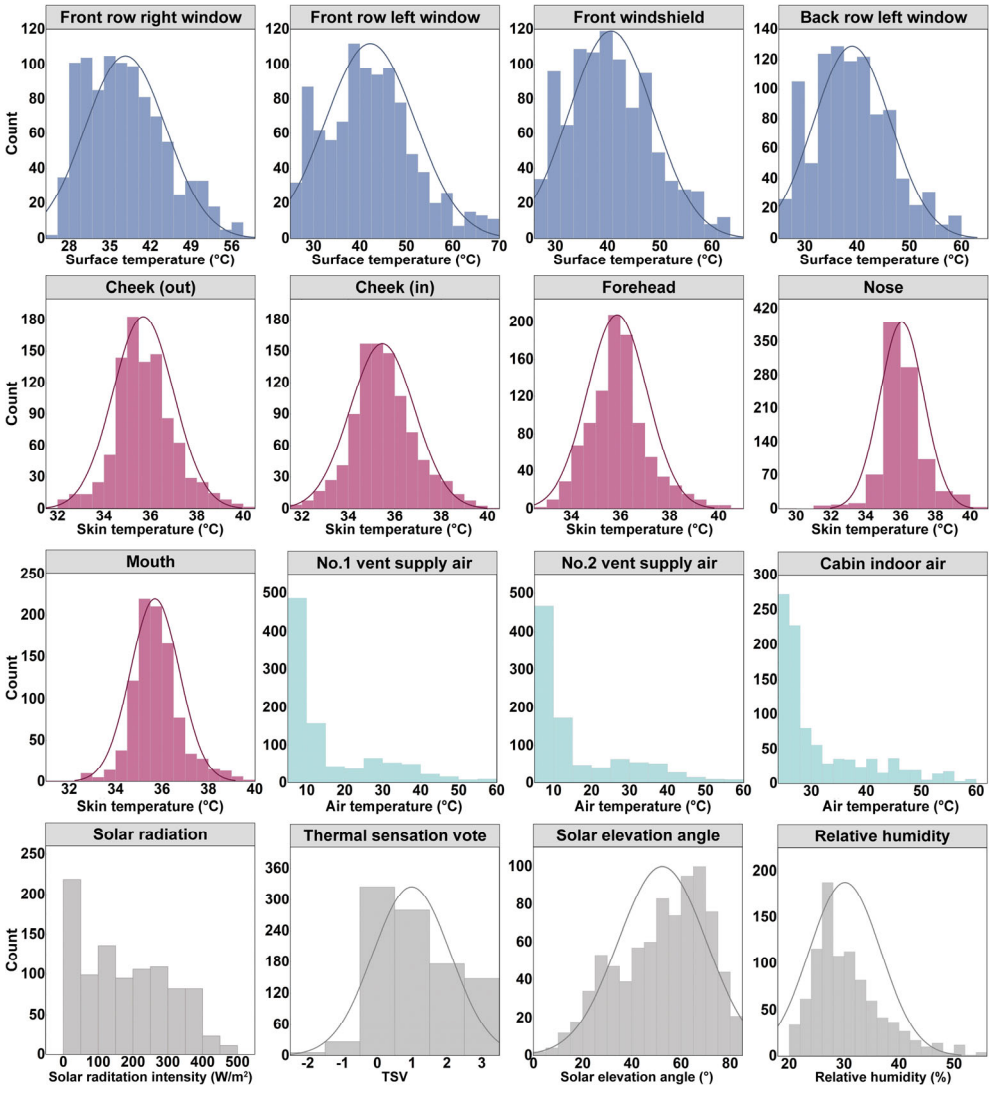

Fig. 4 Statistical distributions of the collected dataset

Table 4 Model feature group divided according to type

Grouping	Type	Parameters included
1	Environmental feature	Sex, SR, SE, Orientation, T_A, $T_{Supply,1}$, $T_{Supply,2}$, T_{RFW}, T_{LFW}, T_{FW}, T_{LBW}
2	Facial skin temperature information	Sex, Orientation, $T_{Cheek(in)}$, $T_{Cheek(out)}$, $T_{Forehead}$, T_{Nose}, T_{Mouth}, T_{STD}, T_{Max}, T_{Min}, T_{ED}, $dT_{Cheek(out)}/dt$, $dT_{Cheek(in)}/dt$, $dT_{Forehead}/dt$, dT_{Nose}/dt, dT_{Mouth}/dt
3	Mixed feature of environmental and facial skin temperature	Sex, SR, SE, Orientation, T_A, $T_{Supply,1}$, $T_{Supply,2}$, T_{RFW}, T_{LFW}, T_{FW}, T_{LBW}, $T_{Cheek(in)}$, $T_{Cheek(out)}$, $T_{Forehead}$, T_{Nose}, T_{Mouth}, T_{STD}, T_{Max}, T_{Min}, T_{ED}, $dT_{Cheek(out)}/dt$, $dT_{Cheek(in)}/dt$, $dT_{Forehead}/dt$, dT_{Nose}/dt, dT_{Mouth}/dt
4	Easily measured feature, application based	Sex, SR, SE, Orientation, T_A, $T_{Supply,1}$, $T_{Supply,2}$, $T_{Cheek(in)}$, $T_{Cheek(out)}$, $T_{Forehead}$, T_{Nose}, T_{Mouth}, T_{STD}, T_{Max}, T_{Min}, T_{ED}, $dT_{Cheek(out)}/dt$, $dT_{Cheek(in)}/dt$, $dT_{Forehead}/dt$, dT_{Nose}/dt, dT_{Mouth}/dt

Grouping 3, Grouping 4 did not include parameters that are difficult to measure in real time with common sensors in actual vehicles, such as the interior surface temperature of the windshield, window surface temperature, etc.

Table 5 lists the performance results of the models established for each feature group using six different algorithms. After comparing the models obtained from various algorithms, it was found that the performance differences are minor except for the decision tree algorithm. Overall, the RFR algorithm shows the lowest MSE and the highest R^2 on the test set, especially under the feature groupings 3 and 4; it also has the highest prediction accuracy on this dataset compared to other algorithms. For the DTR algorithm, the MSE is close to 0, and R^2 is close

Table 5 Comparison of algorithm performance

Feature grouping			LR	RidgeR	LassoR	ENR	DTR	RFR
1	Training set	MSE	0.476	0.477	0.483	0.477	0.001	0.372
		R^2	0.623	0.623	0.618	0.622	0.999	0.705
	Test set	MSE	0.452	0.449	0.442	0.447	0.786	0.434
		R^2	0.606	0.609	0.614	0.610	0.314	0.621
2	Training set	MSE	0.555	0.556	0.569	0.560	0.000	0.212
		R^2	0.561	0.560	0.549	0.556	1.000	0.832
	Test set	MSE	0.639	0.645	0.651	0.644	0.998	0.598
		R^2	0.493	0.488	0.484	0.489	0.208	0.526
3	Training set	MSE	0.412	0.413	0.421	0.417	0.000	0.187
		R^2	0.666	0.666	0.659	0.662	1.000	0.851
	Test set	MSE	0.446	0.439	0.441	0.439	0.738	0.415
		R^2	0.632	0.637	0.636	0.638	0.414	0.661
4	Training set	MSE	0.416	0.417	0.422	0.419	0.000	0.085
		R^2	0.663	0.662	0.658	0.660	1.000	0.931
	Test set	MSE	0.447	0.440	0.441	0.439	0.766	0.438
		R^2	0.631	0.636	0.636	0.638	0.362	0.645

to 1 for training sets; however, its performance significantly decreases on the test set, especially with a lower R^2 score, suggesting that using the DTR algorithm on this dataset has overfitting problem. RFR also performs very well on the training set, but compared to the DTR, its performance on the test set is relatively more stable. LR, RidgeR, LassoR, and ENR show consistent performance on both the training and test sets, indicating they do not have overfitting or underfitting issues and their overall predictive performance is well.

3.3 Thermal sensation assessment model—optimized model

After initial training, the RFR algorithm was found to be the preferred choice for this dataset. Furthermore, by employing the RFECV algorithm, the feature importance for each feature group was ranked, and redundant features were eliminated. This optimized the model's complexity significantly without substantially altering its performance. Figure 5 presents the results of feature selection for different feature groups using RFECV. It illustrates the changes in the MSE of cross-validation as features are incrementally added to the model based on their importance. The right side of the figure lists the features in the order of their importance as determined by the RFECV process. The most critical feature is listed first, followed by the others in sequence. The dashed line in the figure indicates the point where the minimum MSE is reached with the optimal number of features. This suggests that adding more features beyond this point will not significantly improve model performance and may lead to increased model complexity.

For the full environmental parameter feature group, the model achieves stable performance using only four features (T_A, T_{FW}, SR, SE). In terms of the facial skin temperature information feature group, a minimum of six features is required for the model to achieve stable performance, with the maximum facial region skin temperature, nose skin temperature, cheek skin temperature, and the rate of change in nose skin temperature being important features. When combining environmental parameters with facial skin temperature information, the model demonstrates improved performance. A stable performance model can be achieved with seven input features. From a practical application perspective, using air temperature, solar elevation angle, solar radiation intensity, cheek skin temperature, and the standard deviation between facial region skin temperatures, a model with stable performance can be developed and performs well.

After selecting important features for different feature groups, each feature group's corresponding model was retrained and optimized. The model performance is shown in Table 6 (the model number corresponds to the feature group number). Among them, Model 3, which uses environmental parameters and facial skin temperature information as features, exhibits the lowest MSE and the highest R^2 on both the training and test sets, indicating the best performance. However, the features of this model include the surface temperature of the front window. In practice, this is usually not within the measurement scope

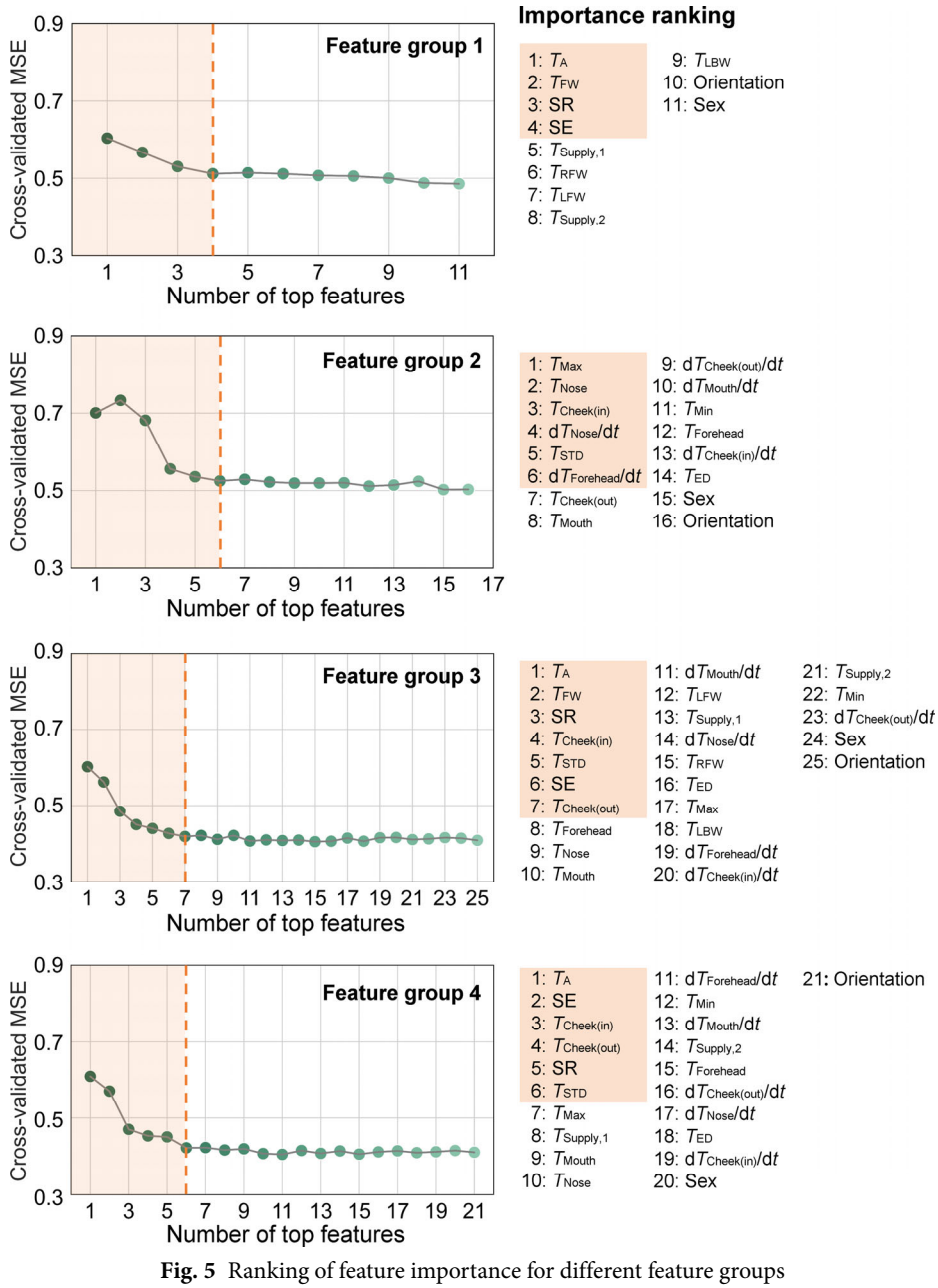

Fig. 5 Ranking of feature importance for different feature groups

Table 6 Model performance after removing redundant features for different feature groups

Model	Adjusted feature	Training set		Test set		Hyperparameter
		MSE	R^2	MSE	R^2	
1	T_A, T_{FW}, SR, SE	0.377	0.702	0.448	0.609	max_depth = 4, n_estimators = 35
2	T_{Max}, T_{Nose}, $T_{Cheek(in)}$, T_{STD}, $dT_{Forehead}/dt$, dT_{Nose}/dt	0.250	0.802	0.599	0.521	max_depth = 8, n_estimators = 17
3	T_A, T_{FW}, T_{STD}, $T_{Cheek(out)}$, SR, $T_{Cheek(in)}$, SE	0.241	0.810	0.422	0.659	max_depth = 6, n_estimators = 11
4	T_A, $T_{Cheek(out)}$, SE, T_{STD}, $T_{Cheek(in)}$, SR	0.243	0.808	0.433	0.651	max_depth = 6, n_estimators = 23

of onboard sensors. Model 4, which is designed from a practical application's perspective, has relative performance as Model 3 while being more feasible. Model 2, which solely uses facial skin temperature information as features, shows the worst performance. This implies that for predicting occupant thermal sensation, it is necessary to comprehensively consider both physiological and environmental parameters to achieve higher accuracy.

3.4 Training set size analysis

Comparison of the impact of training set size on model performance under different models are shown in Figure 6. For the four models trained, when the size of the training set is small, there may not be enough data to capture the true distribution of data, leading to underfitting. As the size of the training set increases, the MSE tends to decreases and the R^2 metric tends to improve. This trend is observed in all the models examined, although the error reduction varies among them. At a training set sample size ratio of 0.5–0.6, most models have relatively lower MSE and higher R^2. Continuing to increase the training set size leads to diminishing returns in model performance improvements. This suggests that the model has likely captured the key features of the data effectively and has not begun overfitting the training set. Further increase in data size may not yield substantial improvements in model performance but would significantly escalate computational and data collection expenses.

4 Validation of the model performance

4.1 Validation experiment

To further validate the generalizability and accuracy of the established model, an independent validation experiment was conducted; separate from the subject experiments used for modeling. This experiment was conducted in Shanghai in September 2023. Given that Model 4, developed from a practical application standpoint, has performance comparable to Model 3, and offers better implement ability, it has been chosen for testing. A total of 12 male subjects were recruited for this validation experiment, comprising both students and staff residing in Shanghai. The study did not impose restrictions on the subjects' age or BMI to evaluate the model's performance across a diverse demographic. To ensure that the experimental outcomes more accurately reflect the model's effectiveness in practical applications, all subjects were recruited spontaneously, and prior to boarding the vehicle, asked to go into an air-conditioned room that is used for everyday work and study. This makes a certain difference than directly going into the experimental chamber with a strictly controlled environment. However, the temporary recruitment of subjects led to variations in experiment durations due to individual scheduling constraints, preventing the establishment of strict baseline duration for the validation experiment. Despite this, all subjects engaged in the experiment for 18–48 min. Specifically, Subjects 1 and 4 were limited to only 18 min of participation because of their other work commitments. Among them, Subjects 1 to 6 were tested in the same vehicle cabin (experimental car #1) used for dataset collection experiment. Subjects 7 and 12 were tested in the cabin of a different small sedan (experimental car #2) to verify the applicability of the established model in various vehicles. Except for Subject 2 and Subject 5 that were tested at night, the rest of the subjects were tested during daytime conditions. Details of each subject and the experimental environment are presented in Table 7. It should be noted that Subjects 2 and 5 underwent their experiments at night, starting with a thermal sensation near neutrality. To assess model performance more effectively in a dynamically changing environment, their cabin environment was initially heated and subsequently cooled. The rest of the subjects conducted their experiments during the daytime, with the air conditioning only set to cooling mode. The real-time air temperature values inside the cabin can be found in Figure S3 in the ESM. After boarding, the subjects voted on thermal sensation and

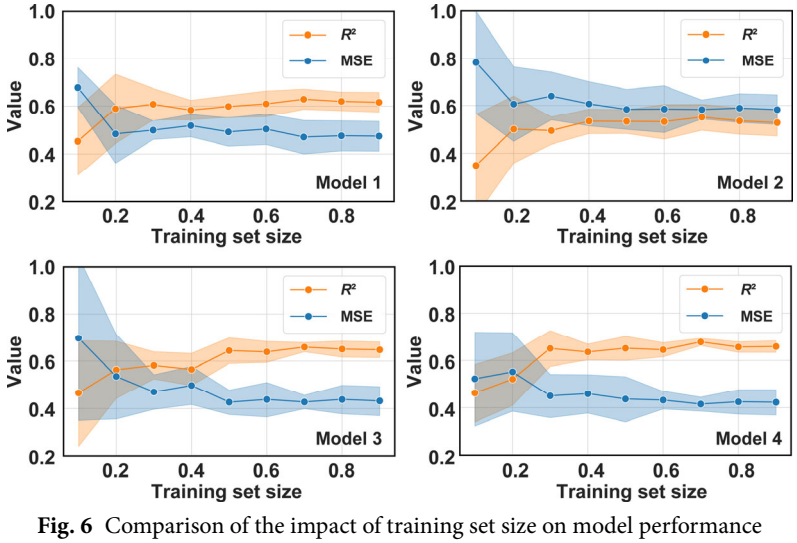

Fig. 6 Comparison of the impact of training set size on model performance

Table 7 Subject information for the validation experiment

	Subject information			Indoor air temperature (°C)				Solar radiation intensity (W/m^2)			
Subject	Age	Weight (kg)	Height (cm)	Mean	Min	Max	SD	Mean	Min	Max	SD
1	30	83	175	28.7	22.5	35.0	3.8	53	37	75	11
2	23	65	180	25.4	19.5	37.0	5.9	0	0	0	0
3	27	68	176	27.2	23.8	33.0	2.5	300	378	269	65
4	28	63	173	30.5	26.0	36.0	3.2	53	37	75	11
5	25	80	185	25.4	18.2	34.0	5.0	0	0	0	0
6	25	82	180	27.3	22.9	34.0	3.5	300	378	269	54
7	24	78	175	28.2	25.5	31.5	2.2	128	90	230	44
8	35	66	175	27.6	25.5	31.0	2.0	132	85	255	57
9	32	80	175	28.3	25.5	34.0	3.0	141	90	262	53
10	27	69	178	26.7	24.0	33.5	3.6	23	10	90	43
11	24	65	175	28.9	26.5	33.5	2.3	125	90	190	29
12	23	68	181	28.8	26.5	33.5	2.3	125	90	190	29

undergo a facial thermal imaging every two minutes. The environmental parameters and facial skin temperature measurement equipment used were consistent with those in the dataset collection experiment.

4.2 Results of the validation experiment

The results of the validation experiment are shown in Figure 7. The results indicate that for most subjects, Model 4 provides a high accuracy in assessing the thermal sensation, with a MAE of 0.37 thermal sensation units for 12 subjects. However, it is also observed that for a small number of individuals, the developed model exhibits significant fluctuations, such as the 9th to 11th votes of Subject 6 and the 15th to 20th votes of Subject 7. This may be because compared to linear regression models, RFR have poorer stability and generalizability. Since RFR cannot accurately make predictions beyond the range of the training set data, this results in larger errors in the predicted values when encountering unseen samples, causing noticeable fluctuations (Savargiv et al. 2021). Furthermore, it was observed in several sessions that the model tends to underestimate the thermal sensation of occupants just after they get on the vehicle, as seen in the cases of subjects 8, 10, 11, and 12. In this research, the model's generalizability was evaluated through validation experiments conducted with sport utility vehicle (SUV) (experimental car #1) for Subjects 1–6, and with a sedan (experimental car #2) for Subjects 7–12. The sedan was reported by the manufacturer to have inferior glass insulation performance—approximately 72% of that of experimental car #1. Consequently, it is expected that the interior surface temperature of experimental car #2 could be higher under similar external environmental conditions. However, Model 4 excludes interior surface temperatures, such as those of the glass and door interiors, from its input features. This exclusion was due to the challenges associated with measuring these parameters and the practical application requirements. This methodological decision introduces a limitation, potentially compromising the model's ability to fully account for the influence of the vehicle's structure on occupants' thermal sensation, particularly in scenarios where the air conditioner is inactive. This could lead to an underestimation of thermal sensation, a hypothesis that aligns with the observations depicted in Figure 7.

5 Discussion

5.1 Model based on facial skin temperature or environmental parameters?

Due to its exposure, facial skin often experiences great fluctuations influenced by environmental changes, making facial skin temperature an indicator for assessing occupant thermal sensations. The fact that the face is usually less covered makes it easy to measure skin temperature using non-contact sensors. Currently, the use of facial skin temperature to establish models for assessing occupant thermal sensation has become a research focus. Nonetheless, these models incorporate not just facial skin temperature but also a range of environmental parameters, including air temperature and air velocity. This is consistent with our research findings. In this study, relying solely on facial skin temperature for assessing thermal sensation proves suboptimal, and it is even less effective compared to models that evaluated using only environmental parameters.

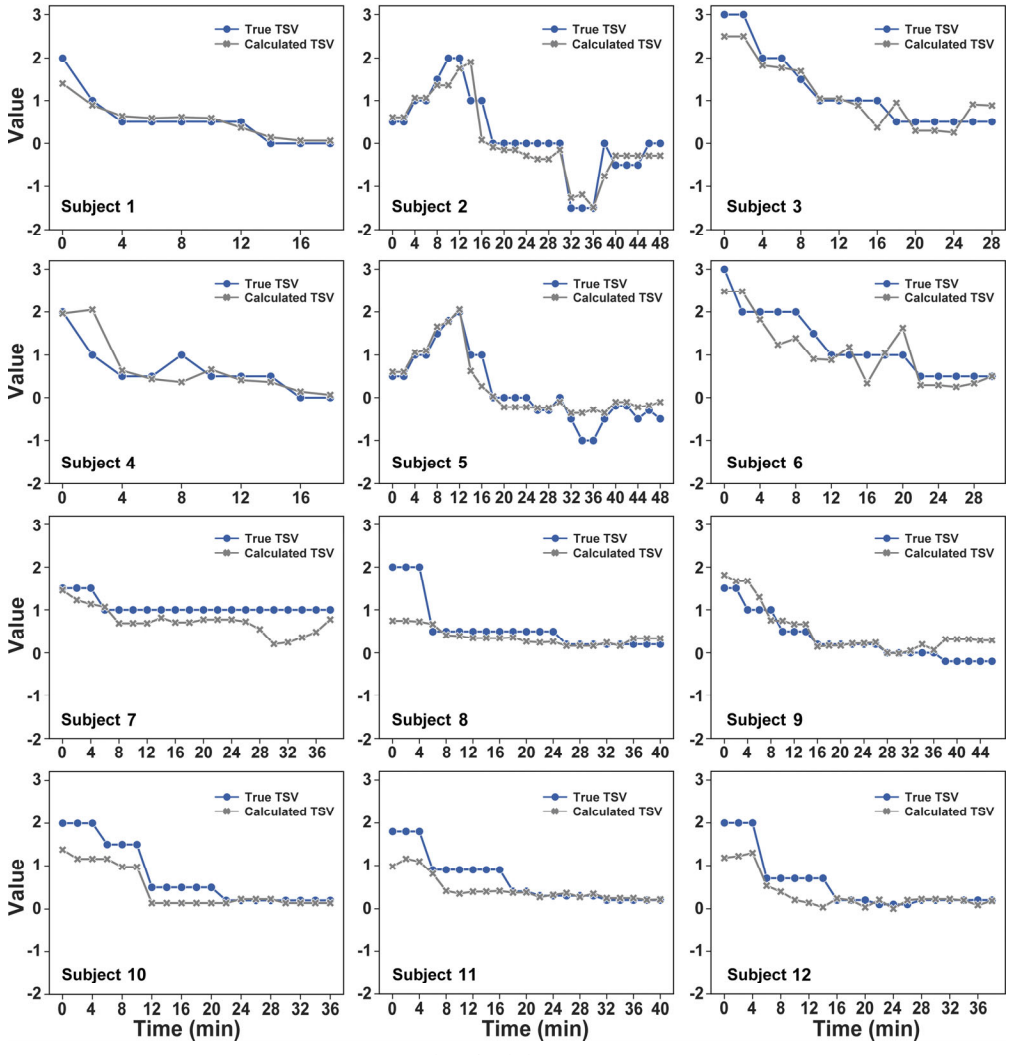

Fig. 7 Results of validation experiment

However, by considering both environmental parameters and facial skin temperature, a marked improvement in the model's performance was noted. Aryal and Becerik-Gerber (2019) indicated the addition of physiological parameter sensors alongside environmental sensors might not be economically viable. They found that using only environmental parameters was sufficient to construct a relatively accurate thermal sensation assessment model. However, this study found that even in cabins with similar environmental parameters, subjects' thermal sensations could vary significantly. Taking sex differences as an example, this study found that in the same environment, the thermal sensation of males could be significantly higher than that of females (see Figure 8). Assessing thermal sensation in individuals who are in the same environment but have individual differences (such as sex, age, BMI, etc.) is difficult to effectively address by only detecting environmental parameters. Facial skin temperature, on the other hand, can more accurately reflect these individual differences.

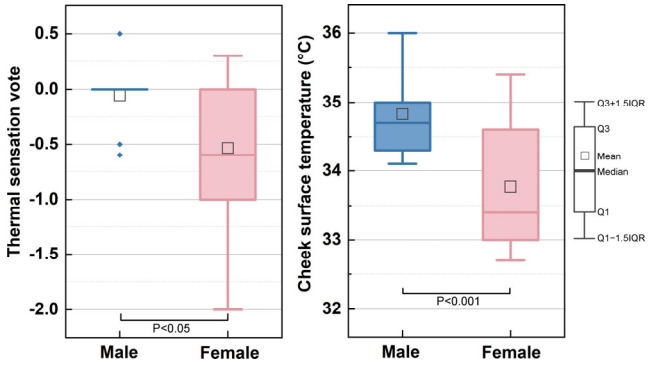

Fig. 8 Steady-state thermal sensation and cheek surface temperature during nighttime experimental condition

Therefore, including physiological parameters as assessment features in the evaluation of thermal sensation in cabin environments is effective. This approach provides a new perspective for addressing individual differences in assessing thermal sensation.

5.2 Challenges in practical application

This study establishes a model for assessing occupant thermal sensation in vehicle cabins. From a practical application perspective, by using solar radiation intensity, cabin air temperature, solar elevation angle, and facial skin temperature data as inputs, it provides a strategy for the individualized automatic control of vehicle A/C. Among these, facial skin temperature information is collected through thermal imaging sensors. However, this needs to be further evaluated from a cost perspective. Wu et al. (2023c) reviewed and summarized the thermal imaging sensors used in related research. Among them, the cheapest sensor is the MLX90640, costing $30. But its resolution is 32 × 24, with an accuracy of ±2 °C. The most expensive thermography costs up to $2,700. Wu et al. (2023b) used the Hikvision DS-2TD3017T-2/V dual-spectrum thermography in their research for facial segmentation and temperature collection. Its cost and performance achieve an ideal balance, but overall, it still amounts to $300. Even though this study found that the assessment performance of occupant thermal sensation can be improved by considering both environmental parameters and facial skin temperature, the application of high-performance thermal imaging sensors in actual environmental control would be greatly limited if the cost of these sensors is too high. Aryal and Becerik-Gerber (2019, 2020) expressed a similar view in their comparative study of automatic control schemes based on indoor thermal environment of buildings, noting that although adding physiological parameters can improve the accuracy of thermal sensation assessment, the increased system costs seems unworthy. However, compared to the control of the indoor environment of buildings, the cabin environment has its unique advantages. On the one hand, due to the narrow space of the cabin, the distance between the thermal imaging sensor and the occupants is reduced. This provides application opportunities for some economical sensors that are high in accuracy but lower in resolution. On the other hand, since the A/C system of the vehicle cabin is integrated into the vehicle itself, installing thermal imaging sensors in the cabin not only enables the collection of skin temperature but can also be used for other purposes such as fatigue monitoring of the driver, and performance monitoring of the vehicle's enclosure structure.

In addition to thermal imaging sensors, solar radiation sensors should also be considered for their cost-effectiveness. Given the current market, commercial-grade solar radiation sensors can be priced at less than $15. Although the price of solar radiation sensors is higher than that of well-developed temperature sensors, in terms of the overall vehicle price, this only constitutes a very small fraction. It's noteworthy that with the electrification transformation of vehicles, an increasing number of cars on the market are now equipped with solar radiation sensors. These sensors not only drive the automatic adjustment of sunshades and windows but also assist in more efficient battery thermal management by analyzing solar radiation in real-time and adjusting energy usage strategies accordingly to extend driving range. With technological advancements, a single sensor is no longer limited to a specific task but can provide essential data collection for the overall operation and regulation of the vehicle. Overall, balancing the relationship between equipment performance and cost to achieve optimal cabin thermal comfort at an acceptable cost remains an issue worth considering when applying this assessment method.

5.3 Limitations

This study developed a thermal sensation assessment model for cabin occupants based on environmental parameters and facial skin temperature information collected through thermal imaging. However, the dataset used for this model was derived from experiments with subjects inside a cabin during the summer. Due to differences in clothing level between winter and summer, as well as the varying directions of radiant heat flow between walls and the human body during these seasons, the model developed for a summer cabin may not be applicable to winter conditions. Furthermore, the thermography used in this study is high-cost professional equipment, making its application difficult in actual vehicle systems. In the future, further exploration is needed for a low-cost thermal sensation assessment system for cabin occupants based on thermal imaging.

6 Conclusion

This study, based on subject experiments, established a summer thermal sensation assessment model for vehicle cabin occupants and conducted performance validation of the established model in independent experiments. The validation confirmed that the model established in this study performs well, with the specific conclusions as follows:

1) Indoor air temperature, windshield surface temperature, the standard deviation of facial skin temperature, cheek skin temperature, solar radiation intensity, and solar elevation angle are important features for establishing a thermal sensation assessment model for vehicle cabin occupants.
2) A model using environmental parameters (indoor air temperature, windshield surface temperature, solar radiation intensity, and solar elevation angle) as well as facial skin temperature information (standard deviation of facial skin temperature, cheek skin temperature)

performing the best. From the perspective of practical application, after eliminating the difficult-to-measure feature of windshield surface temperature, the performance slightly decreased but still performed well, with an R^2 of 0.651 and an MSE of 0.433 on the test set. In independent validation experiments, the MAE was less than 0.4 thermal sensation units.

3) When the sample size of the training set was 481–578, the MSE of the trained models was relatively low, and the R^2 was relatively high. Continuing to enlarge the training size resulted in limited improvement in model performance, while significantly increasing computation and data collection costs.

Electronic Supplementary Material (ESM): Supplementary materials are available in the online version of this article at https://doi.org/10.1007/s12273-024-1147-0.

Acknowledgements

This work is supported by the National Key R&D Program of China (2022YFC3803201).

Declaration of competing interest

The authors have no competing interests to declare that are relevant to the content of this article.

Author contribution statement

All authors contributed to the study conception and design. Material preparation, data collection and analysis were performed by Junmeng Lyu, Yuxin Yang, Yongxiang Shi, Zhiwei Lian. The first draft of the manuscript was written by Junmeng Lyu and all authors commented on previous versions of the manuscript. All authors read and approved the final manuscript.

References

Arens E, Zhang H, Huizenga C (2006a). Partial- and whole-body thermal sensation and comfort: Part I: Uniform environmental conditions. *Journal of Thermal Biology*, 31: 53–59.

Arens E, Zhang H, Huizenga C (2006b). Partial- and whole-body thermal sensation and comfort: Part II: Non-uniform environmental conditions. *Journal of Thermal Biology*, 31: 60–66.

Aryal A, Becerik-Gerber B (2019). A comparative study of predicting individual thermal sensation and satisfaction using wrist-worn temperature sensor, thermal camera and ambient temperature sensor. *Building and Environment*, 160: 106223.

Aryal A, Becerik-Gerber B (2020). Thermal comfort modeling when personalized comfort systems are in use: Comparison of sensing and learning methods. *Building and Environment*, 185: 107316.

Belgiu M, Drăguț L (2016). Random forest in remote sensing: A review of applications and future directions. *ISPRS Journal of Photogrammetry and Remote Sensing*, 114: 24–31.

Choi JH, Loftness V (2012). Investigation of human body skin temperatures as a bio-signal to indicate overall thermal sensations. *Building and Environment*, 58: 258–269.

Cosma AC, Simha R (2018). Thermal comfort modeling in transient conditions using real-time local body temperature extraction with a thermographic camera. *Building and Environment*, 143: 36–47.

de Santis M, Silvestri L, Forcina A (2022). Promoting electric vehicle demand in Europe: Design of innovative electricity consumption simulator and subsidy strategies based on well-to-wheel analysis. *Energy Conversion and Management*, 270: 116279.

Fanger PO (1970). Thermal Comfort: Analysis and Applications in Environmental Engineering. Copenhagen: Danish Technical Press.

Fiala D, Lomas KJ, Stohrer M (2003). First principles modeling of thermal sensation responses in steady-state and transient conditions. *ASHRAE Transactions*, 109(1): 179–186.

Guan Y, Hosni MH, Jones BW, et al. (2003a). Investigation of human thermal comfort under highly transient conditions for automotive applications-Part 1: Experimental design and human subject testing implementation. *ASHRAE Transactions*, 109(2), 885–897.

Guan Y, Hosni MH, Jones BW, et al. (2003b). Investigation of human thermal comfort under highly transient conditions for automotive applications-Part 2: Thermal sensation modeling. *ASHRAE Transactions*, 109(2): 898–907.

Guyon I, Weston J, Barnhill S, et al. (2002). Gene selection for cancer classification using support vector machines. *Machine Learning*, 46: 389–422.

He Y, Zhang H, Arens E, et al. (2023a). Smart detection of indoor occupant thermal state via infrared thermography, computer vision, and machine learning. *Building and Environment*, 228: 109811.

He X, Zhang X, Zhang R, et al. (2023b). More intelligent and efficient thermal environment management: A hybrid model for occupant-centric thermal comfort monitoring in vehicle cabins. *Building and Environment*, 228: 109866.

ISO/TS (2006). ISO 14505-3: 2006 Ergonomics of the Thermal Environment—Evaluation of Thermal Environments in Vehicles - Part 3: Evaluation of Thermal Comfort Using Human Subjects. Geneva, Switzerland: International Organization for Standardization.

Lai D, Zhou X, Chen Q (2017). Modelling dynamic thermal sensation of human subjects in outdoor environments. *Energy and Buildings*, 149: 16–25.

Lai D, Lian Z, Liu W, et al. (2020). A comprehensive review of thermal comfort studies in urban open spaces. *Science of the Total Environment*, 742: 140092.

Lan L, Tang J, Wargocki P, et al. (2022). Cognitive performance was reduced by higher air temperature even when thermal comfort was maintained over the 24–28°C range. *Indoor Air*, 32: e12916.

Li D, Menassa CC, Kamat VR (2018). Non-intrusive interpretation of human thermal comfort through analysis of facial infrared thermography. *Energy and Buildings*, 176: 246–261.

Li D, Menassa CC, Kamat VR (2019). Robust non-intrusive interpretation of occupant thermal comfort in built environments with low-cost networked thermal cameras. *Applied Energy*, 251: 113336.

Li W, Chen J, Lan F, et al. (2022). Human thermal sensation and its algorithmic modelization under dynamic environmental thermal characteristics of vehicle cabin. *Indoor Air*, 32: e13168.

Lian Z (2024). Revisiting thermal comfort and thermal sensation. *Building Simulation*, 17: 185–188.

Lyu J, Du H, Zhao Z, et al. (2023). Where should the thermal image sensor of a smart A/C look? -Occupant thermal sensation model based on thermal imaging data. *Building and Environment*, 239: 110405.

Mustaqim AZ, Adi S, Pristyanto Y, et al. (2021). The effect of Recursive Feature Elimination with Cross-Validation (RFECV) feature selection algorithm toward classifier performance on credit card fraud detection. In: Proceedings of the 2021 International Conference on Artificial Intelligence and Computer Science Technology (ICAICST), Yogyakarta, Indonesia.

Nadel ER, Bullard RW, Stolwijk JA (1971). Importance of skin temperature in the regulation of sweating. *Journal of Applied Physiology*, 31: 80–87.

Pedregosa F, Varoquaux G, Gramfort A, et al. (2011). Scikit-learn: Machine learning in python. *Journal of Machine Learning Research*, 12: 2825–2830.

Qavidel Fard Z, Zomorodian ZS, Korsavi SS (2022). Application of machine learning in thermal comfort studies: A review of methods, performance and challenges. *Energy and Buildings*, 256: 111771.

Savargiv M, Masoumi B, Keyvanpour MR (2021). A new random forest algorithm based on learning automata. *Computational Intelligence and Neuroscience*, 2021: 5572781.

Shan X, Yang EH (2020). Supervised machine learning of thermal comfort under different indoor temperatures using EEG measurements. *Energy and Buildings*, 225: 110305.

Sun R, Liu J, Lai D, et al. (2023). Building form and outdoor thermal comfort: Inverse design the microclimate of outdoor space for a kindergarten. *Energy and Buildings*, 284: 112824.

Wang Z, Wang J, He Y, et al. (2020). Dimension analysis of subjective thermal comfort metrics based on ASHRAE Global Thermal Comfort Database using machine learning. *Journal of Building Engineering*, 29: 101120.

Wu Z, Li N, Peng J, et al. (2018). Using an ensemble machine learning methodology—Bagging to predict occupants' thermal comfort in buildings. *Energy and Buildings*, 173: 117–127.

Wu Y, Cao B (2022). Recognition and prediction of individual thermal comfort requirement based on local skin temperature. *Journal of Building Engineering*, 49: 104025.

Wu Y, Cao B, Hu M, et al. (2023a). Development of personal comfort model and its use in the control of air conditioner. *Energy and Buildings*, 285: 112900.

Wu Y, Cao B, Zhu Y (2023b). Development of an automatic personal comfort system (APCS) based on real-time thermal sensation prediction. *Building and Environment*, 246: 110958.

Wu Y, Zhao J, Cao B (2023c). A systematic review of research on personal thermal comfort using infrared technology. *Energy and Buildings*, 301: 113666.

Yang B, Cheng X, Dai D, et al. (2019). Real-time and contactless measurements of thermal discomfort based on human poses for energy efficient control of buildings. *Building and Environment*, 162: 106284.

Yang B, Li X, Hou Y, et al. (2020). Non-invasive (non-contact) measurements of human thermal physiology signals and thermal comfort/discomfort poses-A review. *Energy and Buildings*, 224: 110261.

Zhang H. (2003). Human thermal sensation and comfort in transient and non-uniform thermal environments. PhD Thesis, University of California, Berkeley, USA.

Zhang H, Arens E, Huizenga C, et al. (2010a). Thermal sensation and comfort models for non-uniform and transient environments: Part I: Local sensation of individual body parts. *Building and Environment*, 45: 380–388.

Zhang H, Arens E, Huizenga C, et al. (2010b). Thermal sensation and comfort models for non-uniform and transient environments, part III: Whole-body sensation and comfort. *Building and Environment*, 45: 399–410.

Zhao Q, Lian Z, Lai D (2021). Thermal comfort models and their developments: A review. *Energy and Built Environment*, 2: 21–33.

Zhao Q, Lyu J, Du H, et al. (2023). Gender differences in thermal sensation and skin temperature sensitivity under local cooling. *Journal of Thermal Biology*, 111: 103401.

Zhou X, Lai D, Chen Q (2020). Thermal sensation model for driver in a passenger car with changing solar radiation. *Building and Environment*, 183: 107219.